Advanced magneto-optical microscopy: Imaging from picoseconds to centimeters - imaging spin waves and temperature distributions (invited)

Necdet Onur Urs, Babak Mozooni, Piotr Mazalski, Mikhail Kustov, Patrick Hayes, Shayan Deldar, Eckhard Quandt, and Jeffrey McCord

Citation: AIP Advances **6**, 055605 (2016); doi: 10.1063/1.4943760
View online: http://dx.doi.org/10.1063/1.4943760
View Table of Contents: http://scitation.aip.org/content/aip/journal/adva/6/5?ver=pdfcov
Published by the AIP Publishing

Advanced magneto-optical microscopy: Imaging from picoseconds to centimeters - imaging spin waves and temperature distributions (invited)

Necdet Onur Urs,[1] Babak Mozooni,[1] Piotr Mazalski,[2,3] Mikhail Kustov,[1] Patrick Hayes,[4] Shayan Deldar,[1] Eckhard Quandt,[4] and Jeffrey McCord[1,a]
[1]*Nanoscale Magnetic Materials - Magnetic Domains, Institute for Materials Science, Kiel University, Kiel, Germany*
[2]*Faculty of Physics, University of Białystok, Białystok, Poland*
[3]*Jerzy Haber Institute of Catalysis and Surface Chemistry, Polish Academy of Sciences, Kraków, Poland*
[4]*Inorganic Functional Materials, Institute for Materials Science, Kiel University, Kiel, Germany*

(Presented 15 January 2016; received 6 November 2015; accepted 15 December 2015; published online 8 March 2016)

Recent developments in the observation of magnetic domains and domain walls by wide-field optical microscopy based on the magneto-optical Kerr, Faraday, Voigt, and Gradient effect are reviewed. Emphasis is given to the existence of higher order magneto-optical effects for advanced magnetic imaging. Fundamental concepts and advances in methodology are discussed that allow for imaging of magnetic domains on various length and time scales. Time-resolved imaging of electric field induced domain wall rotation is shown. Visualization of magnetization dynamics down to picosecond temporal resolution for the imaging of spin-waves and magneto-optical multi-effect domain imaging techniques for obtaining vectorial information are demonstrated. Beyond conventional domain imaging, the use of a magneto-optical indicator technique for local temperature sensing is shown. [http://dx.doi.org/10.1063/1.4943760]

I. INTRODUCTION

The imaging of magnetic domain structures in magnetic materials and devices is of high importance to understand and thus optimize the magnetization behavior in magnetic bulk and film structures. Magnetic domain imaging gives indispensable information on the mechanisms of magnetic reversal behavior in magnetic samples and provides clarification of the origin of effective magnetic properties. Numerous techniques for obtaining spatially resolved data associated to the distribution of magnetization inside magnetic materials are existing, each of them with their specific advantages and shortcomings. Reviews on various magnetic domain observation techniques including recent developments are given in Refs. 1–3.

From an application point of view, existing methods differ in terms of attainable spatial and temporal resolution, and in terms of image acquisition times due to full field imaging versus scanning techniques. Magneto-optical (MO) microscopy is a well-established laboratory technique that allows for multiple imaging options.[1,4] In most cases the imaging is based on the so-called linear MO effects, which are the MO Kerr effect in reflection and the MO Faraday effect in transmission using wavelengths in the visible spectra. Nevertheless, 2nd order MO effects additionally contribute to image formation.

Here we review the latest developments in MO wide-field imaging of magnetic domains with different fields of view varying by about four orders of magnitude and on very short time scales.

[a]jmc@tf.uni-kiel.de; http://www.tf.uni-kiel.de/nmm/en

Special attention is given to the simultaneously occurring primary and secondary MO effects. The versatility of MO imaging is further demonstrated, discussing an alternative application of MO imaging beyond traditional magnetic domain imaging.

II. MICROSCOPE SETUPS

Two dissimilar basic configurations of wide-field MO domain imaging microscopes are available. One arrangement is most suitable for MO Kerr effect (MOKE) microscopy of large samples with an in-plane alignment of magnetization. The other kind of setup is an adapted polarized light microscope and is suited for MO effect domain observations with high magnification and high spatial resolution. A general advantage of wide-field MO microscopy over scanning microscopy methods is the direct imaging scheme by which the exposure time becomes decoupled from sample size and applied magnification.

MOKE microscopy at low magnification and with a field of view of up to several centimeters is possible by using a setup consisting of an inclined microscope for the observation and a equally tilted detached illuminating system (Fig. 1(a)). Through the tilted axis of illumination and observation (tilted by θ_{inc}) MO observations with an oblique plane of incidence are possible. The large angle of incidence needed for the imaging of in-plane magnetizations by longitudinal MOKE can be obtained. Significant in-plane sensitive longitudinal MOKE contrast is realized even for low optical magnifications (Fig. 1(b)). Effects of image distortion and problems with the depth of focus are eliminated by a Scheimpflug arrangement with telecentric optics.[4]

The imaging of magnetic domains with varying plane of incidence through a single objective lens is attainable with an adapted polarizing or materials microscope.[1,4] The setup allows for imaging with a spatial resolution down to approximately 200 nm. Imaging of in-plane magnetic domains with the longitudinal MOKE works best with high numerical aperture (NA) objective lenses. The principle ray diagram of an advanced MO imaging setup with different kinds of illumination sources and detection schemes is sketched in Fig. 2(a). The general scheme of operation is described in detail in Ref. 4.

With the latest developments of illumination sources advanced imaging schemes are possible. Interchangeable light sources include high-power light emitting diodes (LEDs) and lasers. Both allow for imaging with temporal resolution, for the laser down to picosecond time scales. For very fast imaging schemes stroboscopic image schemes are applied. Using multiple illumination sources

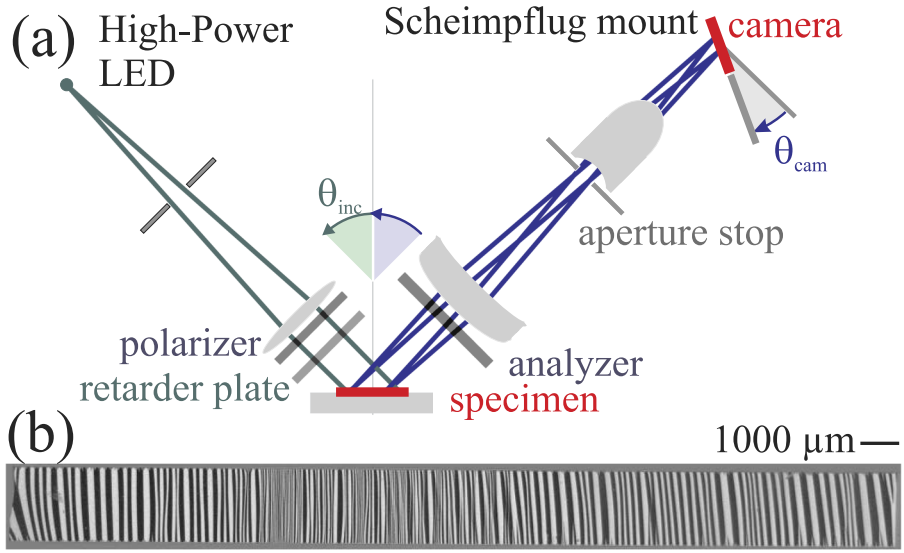

FIG. 1. (a) Scheme of a large view microscope for the imaging of in-plane magnetic domains. Undistorted imaging is achieved using bi-axial telecentric lenses in conjunction with Scheimpflug optics (sketch after Ref. 4). (b) Exemplary longitudinal MOKE image of a magneto-electric sensor structure with centimeter dimensions.

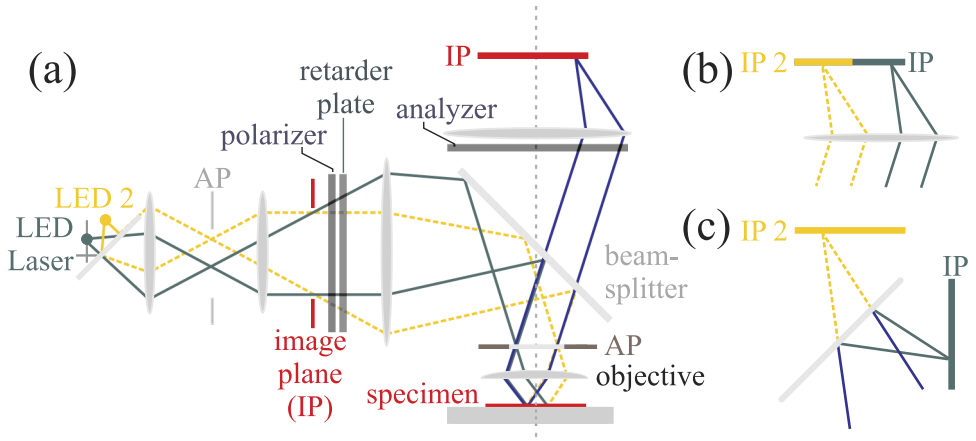

FIG. 2. (a) Scheme of a high resolution optical MO effect microscope with an interchangeable single LED, multiple LEDs (LED and LED1), or pulsed Laser illumination. Image separation for multi-component microscopy can be achieved by different means using (b) an image splitter[4] or (c) a dual camera detection scheme.[5]

concurrently, the simultaneous imaging with two or more different MO effects is possible. Yet, this requires a way of separating the image paths for observation. This is achievable by the application of two synchronized cameras[5] or an image-splitter, where the divided image is then captured by a single camera[4] (Fig. 2(b) and 2(c)).

III. MAGNETO-OPTICAL EFFECTS IN MO MICROSCOPY

Magneto-optical domain observations in reflection and transmission are mainly based on magnetic circular birefringence. The MO effects that are odd in magnetization M ($\sim M$) include the magneto-optical Faraday effect (MOFE) in transmission and the magneto-optical Kerr effect (MOKE) in reflection. Depending on the orientation of M relative to the plane of incidence and the orientation of the polarization of light, three fundamental types of MO geometries are defined: longitudinal and polar MOFE and MOKE, and transverse MOKE. The transverse effect only occurs in reflection.

Infrequently, magnetic linear birefringence is used for the imaging of magnetic domains. The magneto-optical Voigt effect (MOVE) is even in M ($\sim M^2$). Yet, the obtained MOVE signal is weak relative to the MOKE effect. It is used in the polar MO geometry for in-plane magnetized films, where the longitudinal MOKE is zero. In contrast to MOKE imaging, it allows for the imaging of magnetic structures with in-plane alignment of magnetization but with perpendicular incidence of light. MOFE, MOKE, and MOVE have their origin in spin-orbit and exchange interactions, where the MOFE and the MOKE rely on first order and the MOVE on second order spin-orbit coupling. As the 2nd order contributions of spin-orbit coupling are typically significantly smaller than the 1st order contributions, therefore the MOVE is usually much weaker than the 1st order MO effects. A list of the relevant MO phenomena with its dependency on M ($f(M)$) is given in Table I. With the microscope extensions described in sect. I the simultaneous and reproducible use of two MO effects becomes attainable.

TABLE I. Magneto-optical phenomena.

Physical phenomena	$f(M)$
Magnetic circular birefringence (MOFE, MOKE)	linear
Magnetic circular dichroism	linear
Magnetic linear birefringence (MOVE)	quadratic
Magnetic linear dichroism	quadratic
Gradient contrast (MOGE)	differential

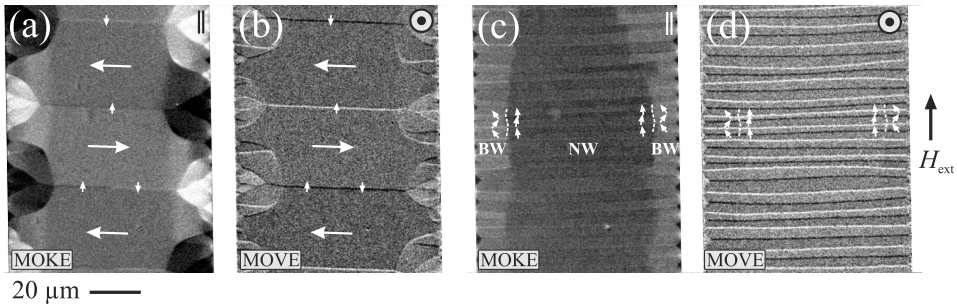

FIG. 3. Complementary (a) MOKE and (b) MOVE image of a magnetic domain state after demagnetizing along the easy axis of magnetization. Magnetic domain configuration at $H_{ext} = 1.2$ Oe (as indicated) for (c) MOKE and (d) MOVE geometry. The region with Bloch walls (BW) and Néel walls (NW) are marked. The plane of oblique incidence for MOKE (‖) and the perpendicular incidence for MOVE (⊙) imaging are indicated (sample: single layer $Co_{40}Fe_{40}B_{20}$, thickness 160 nm).

An example of the information obtainable on magnetic domains and domain walls from complementary MOKE and MOVE imaging is shown in Fig. 3. Fig. 3(a) displays a MOKE image of a single layer $Co_{40}Fe_{40}B_{20}$ film structure that was demagnetized along its easy axis of magnetization. The MOKE sensitivity is adjusted in order to probe the asymmetric Bloch-type magnetic domain walls, separating magnetic domains in the middle of the structure. Bloch wall segments with opposite MOKE contrast, separated by Bloch lines are visible. In Fig. 3(b) the obtained magnetic domain image in MOVE geometry is shown. Regions with antiparallel alignment of magnetization directions show the same MOVE contrast. Moreover, in the MOVE geometry the MO gradient effect (MOGE)[6] can be probed, which is observed as an alternating domain boundary contrast in Fig. 3(b). The effect can be derived by classical magneto-optical diffraction theory, by which its amplitude is proportional to the 1st order MO effects. It is assumed to be caused only by a gradient of magnetization. Fig. 3(c) displays the magnetic domain configuration at a small bias field H_{ext}. Due to the varying internal field two types of domain walls co-exist. Asymmetric Néel-type magnetic domain walls are additionally formed in the central part of the element. The related tilting of magnetization due to the interacting Néel-wall tails contributes to the central MOKE contrast. Imaging the domain configuration in MOVE geometry Fig. 3(d), the magnetic domains with collinear alignment of magnetization display equal MOVE contrast. However, most noticeably a uniform and alternating MOGE contrast is observed for all magnetic domain boundaries. None of the domain wall transitions are visible, indicating that the MOGE is not influenced by the internal structure of the domain walls. This indicates that the MOGE is insensitive to the domain wall structure as suggested in Ref. 7. The MOGE appears to be defined by the gradient of magnetization across the domain boundaries.

A concluding proof of the MOGE behavior is obtained by imaging of compensated surface domain walls by means of simultaneous multi-effect MO imaging, involving MOKE, MOVE, and MOGE imaging. The same magnetic domain configurations are imaged by two orthogonal MOKE sensitivities and in MOVE geometry. In the experiment, zero degree magnetic domain walls are generated in the magnetic multi-layer structure that display no gradient of magnetization across the domain boundary. In Fig. 4 magnetic domain configurations of an exchange biased bilayer with opposite sign of exchange bias for the individual layers are displayed. The essential magnetic layer structure is Ta (5nm)/ NiFe (2.5 nm)/ IrMn (7 nm)/ $CoFeB_{\rightarrow}$ (80 nm)/ Ta (5nm)/ NiFe (2.5 nm)/ IrMn (7 nm)/ $CoFeB_{\leftarrow}$ (80 nm)/ TaN (3nm) (CoFeB = $Co_{40}Fe_{40}B_{20}$; NiFe = $Ni_{81}Fe_{19}$). The top ferromagnetic CoFeB layer (t_{fm} = 80 nm) is much thicker than the penetration depth of light ($t_{pd} \approx 30$ nm). Hence only the magnetization of the top layer is probed magneto-optically and the bottom ferromagnetic layer is invisible to MO imaging. With the magnetic field opposite to the exchange bias field $H_{eb,top}$ of the top magnetic layer, magnetic domains and domain walls in the top layer become visible in the MOKE images (Fig. 4(a) and 4(b)). The invisible bottom layer is homogeneously magnetized (sketched in Fig. 4(c)). A magnetization loop obtained from the magnetic stack is displayed in Fig. 4(i). Despite the occurrence of domain wall transitions, in the corresponding MOVE and MOGE image (Fig. 4(d)) a homogeneous and alternating boundary contrast is observed. This result is consistent with the data displayed in Fig. 3.

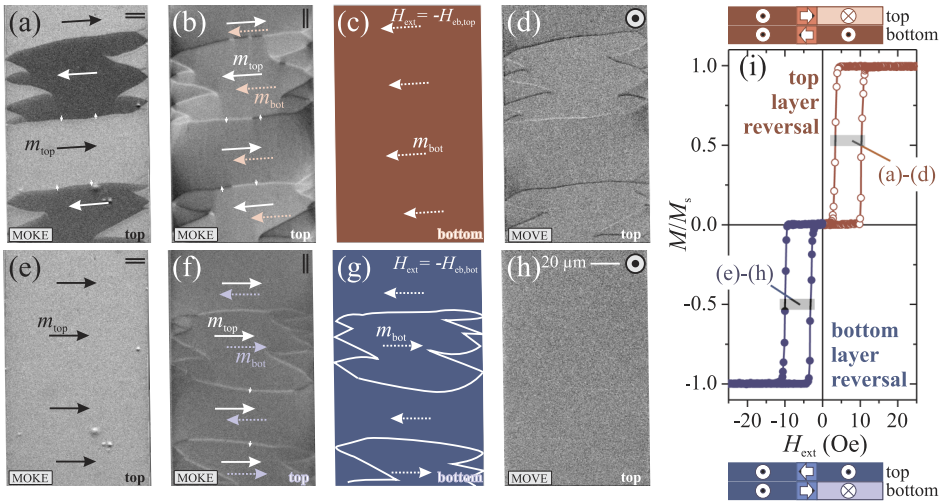

FIG. 4. Complementary magnetic domain images from the top layer of an exchange biased bilayer structure with anti-parallel alignment of exchange bias at (a)-(d) $H_{ext} = -H_{eb,top}$, where the top ferromagnetic layer is in a multi-domain state. In (e)-(h) at $H_{ext} = -H_{eb,bottom}$ the optically invisible bottom layer is in the multi-domain state. In (a) and (e), respectively in (b) and (f) images are obtained with horizontal and vertical MOKE sensitivity. In (d) and (h) MOVE geometry is used for imaging. The magnetization loop of the full film sample and principle sketches of the domain wall structures are displayed in (i). The points in the magnetization loop corresponding to (a)-(d) and (e)-(h) are labeled in (i). The planes of oblique incidence (‖ and =) and perpendicular incidence (⊙) imaging modes are indicated (sample: NiFe (2.5 nm)/ IrMn (7 nm)/ $Co_{40}Fe_{40}B_{20}$ (80 nm)/ Ta (3 nm)/ NiFe (2.5 nm)/ IrMn (7 nm)/ $Co_{40}Fe_{40}B_{20}$ (80 nm)/ Ta (3 nm)).

Yet, aligning H_{ext} opposite to $H_{eb,bottom}$ of the ferromagnetic bottom layer, magnetic domains are now generated in the optically invisible bottom layer. The magnetic top layer is nearly saturated (Fig. 4(e)). Aligning the MOKE sensitivity orthogonally, an imprinting of the bottom layer magnetic domain wall structures becomes visible in the top layer (compare Fig. 4(f)), as now the invisible bottom layer is in a multi-domain state (sketched in Fig. 4(g)). Compensating magnetic 0° domain wall structures form in the top layer to minimize the domain wall energy through magnetostatic interaction. Principle sketches of the occurring compensating domain wall structures are given in Fig. 4(i). Most noticeably, the domain wall structures display no change in magnetization on either side of the wall in the top layer. The effects of domain boundaries and magnetization gradient are thus untangled. No gradient of magnetization exists across the domain wall. As a result, imaging the same magnetic domain (wall) configuration in MOVE geometry displays no MOGE contrast (Fig. 4(h)) (also compare to Fig. 4(d)). This observation eventually clarifies that the MOGE is a pure magnetization boundary effect. MOGE is not originating from magnetic domain walls per se.

IV. MULTI-PATH MAGNETO-OPTICAL IMAGING

The use of a divided optical illumination and observation path (see Fig. 2) enables the direct extraction of different magnetic informations. Multi-path imaging approaches facilitate complicated imaging schemes, involving multiple applied MO sensitivity conditions for the quantitative evaluation of magnetization distributions from one magnetic pattern and separation of in-plane and out-of-plane magnetization components.

A. Quantitative real-time domain imaging

Quantitative imaging using a dual-path microscope is demonstrated in Fig. 5. A pair of complementary magnetic domain images obtained from an epitaxial Fe film with cubic anisotropy is shown in Fig. 5(a) and 5(b). The images, with orthogonal alignment of longitudinal MOKE sensitivity, display corresponding magnetic information of the same magnetic configuration. The derived angular magnetization map is displayed in Fig. 5(c). The example image proves the general

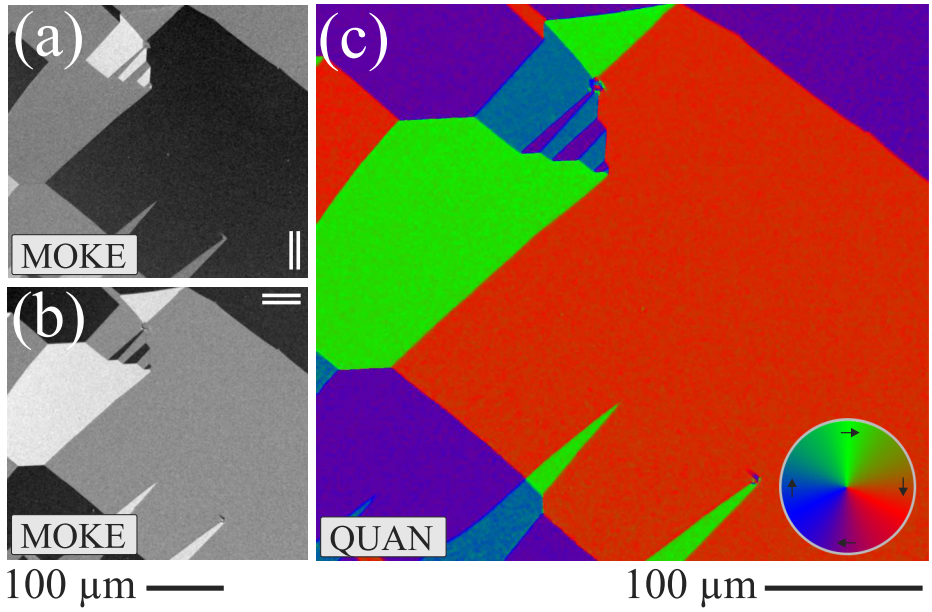

FIG. 5. Longitudinal MOKE images with (a) vertical (||) and (b) horizontal alignment of MO sensitivity (=). (c) Quantitative MO image derived from (a) and (b). The angular distribution of $\boldsymbol{M}$ is color coded as indicated in the inset (sample GaAs/Fe(1 nm)/Ag (150 nm)/Fe (50 nm)/ZnS, courtesy of D. Bürgler, FZ Jülich, after Ref. 5).

feasibility of the dual-path domain imaging technique for quantitative real-time observation, which was already used for the investigation of domain formation in magneto-electric sensor devices.[4,5]

B. Separation of longitudinal and polar MOKE

Dual sensitivity MO imaging can be extended to the separation of in-plane and out-of-plane magnetic contrast in oblique plane of anisotropy films. The separation of magnetization components in locally ion-irradiated Pt/Co/Pt-multilayer structures[8] with as-prepared in-plane anisotropy is shown in Fig. 6. Displayed are images obtained from an ion-irradiated square element. Changing the plane of incidence, differently contrasted MOKE images are obtained (Fig. 6(a) and 6(b)). By addition and subtraction of the MOKE images from opposite oblique plane of incidence, a pure polar (Fig. 6(c)) and, respectively, a pure longitudinal image (Fig. 6(d)) are obtained. Out-of-plane and in-plane components are imaged separately. The latter is not possible by conventional MO microscopy. The data clearly proves the existence of oblique magnetic anisotropy. An estimation of the angle of magnetization from the domain images is possible by comparing the polar and longitudinal magnetic domain contrast (Fig. 6(e)) to the change of MO sensitivity, respectively the ratio of polar-to-longitudinal MO contrast variation with NA of illumination and out-of-plane tilting of magnetization (Fig. 6(f)). From this only a small out-of-plane angle of magnetization of a few degrees at maximum is estimated for the sample displayed in Fig. 6. Due to unequal contributions of polar and longitudinal MOKE signals in image formation, already small out-of-plane components dominate the magnetic image. In comparison to magnetometry data, the MOKE separation method gives rise to the possibility of identification of equilibrium magnetization distribution angles, which are not accessible by integral measurement techniques.

V. IMAGING DYNAMIC MAGNETIZATION PROCESSES

A. Electric field induced dynamics - kHz dynamics

For 2-2 piezoelectric-magnetostrictive composite magneto-electric sensors in cantilever design, the sensor response is amplified at the cantilevers mechanical resonance frequency, which is in the sub- to mid-kHz regime.[9,10] In sensor operation an external magnetic or electric modulation field

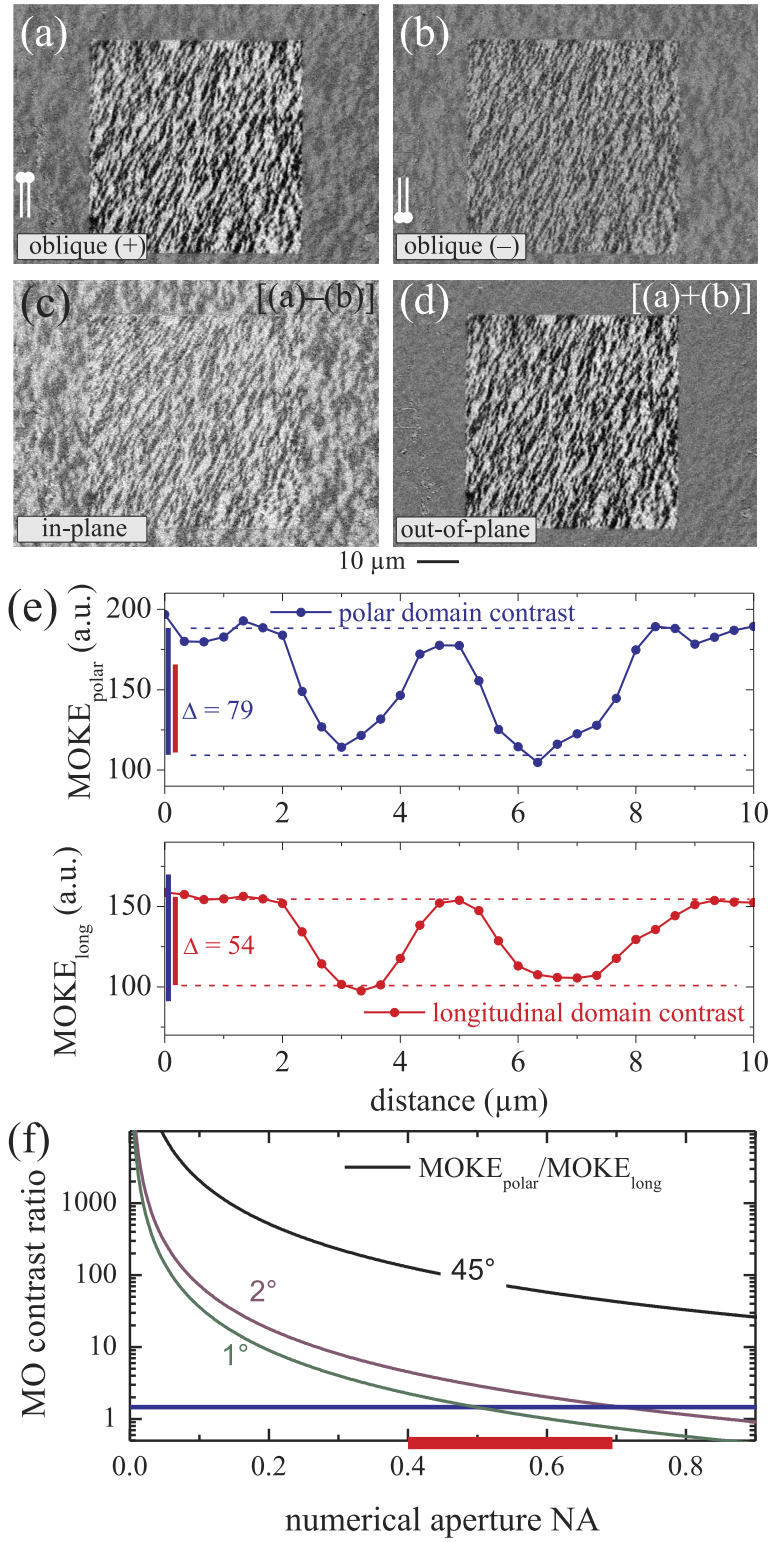

FIG. 6. (a), (b) Magnetic domain images obtained along the same plane of incidence but opposite angle of incidence.[4] (c) Derived pure longitudinal (in-plane, [(a)-(b)]) and (d) pure polar (out-of-plane, [(a)+(b)] MO image. (e) Polar and longitudinal magnetic domain contrast derived from line plots across magnetic domain boundaries from (c) and (d). Polar-to-longitudinal contrast ratio $MOKE_{polar}/MOKE_{longitudinal}$ versus numerical aperture NA and with varying angle of magnetization (1°, 2°, and 45°) relative to the film plane. The region of used NA in (a) and (b) is marked in (c). The planes of incidence are marked in (a) and (b). (sample: Al_2O_3/Mo(20nm)/Pt(20nm)/Co(3.3nm)/Pt(5nm)).

is applied for out-of-resonance measurements.[11] However, due to the modulation field, Barkhausen noise can add to the sensor signal.[5,12] Insight into the underlying magnetic domain mechanism can be gained by time-resolved MOKE experiments at the sensor's mechanical resonance frequency. Fig. 7 displays exemplary images of magnetization response, including domain wall response, of a

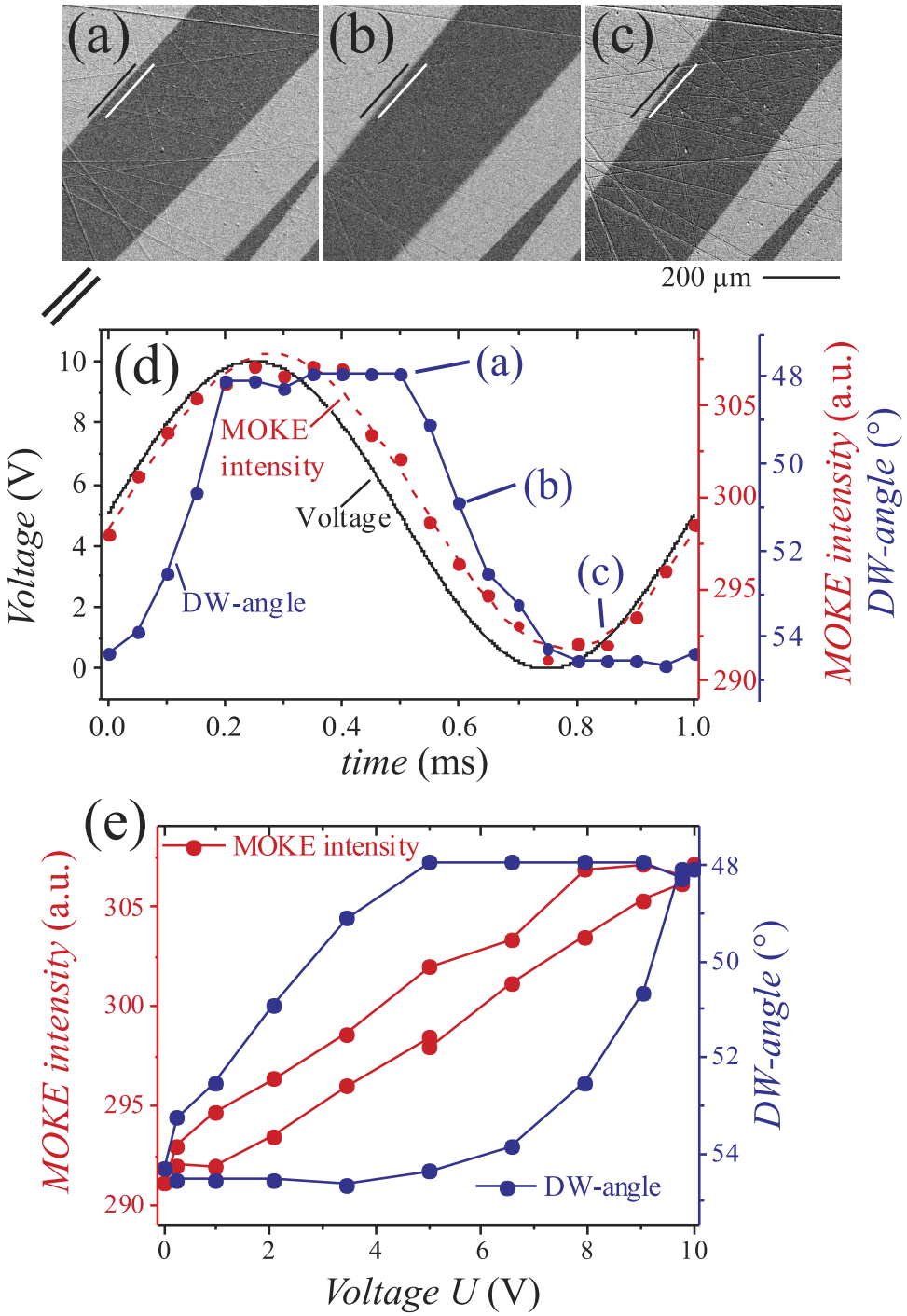

FIG. 7. (a-c) Selected magnetic domain images during electric modulation. (d) The temporal change of MOKE intensity, domain wall angle, and the applied voltage are displayed. (e) The extent of the hysteretic change in domain wall angle and MOKE intensity is shown with respect to the applied voltage. The tilted plane of oblique incidence is indicated underneath (a) (sample: Ta (5 nm)/ FeCoSiB (2 μm)/ Ta (10 nm)/ Si (300 μm)/ PZT (2 μm)).

sensor driven by electric field excitation. A time varying 1 kHz sinusoidal voltage signal of 10 V peak-to-peak amplitude (5 V offset) is applied to the piezoelectric material. The magnetic response in the magnetostrictive layer that results from the electrically induced stress is imaged stroboscopically with a pulsed LED illumination. The temporal resolution of the measurement is 50 μs. The magnetic domain images in Fig. 7(a)-7(c) show the degree of magnetic domain wall rotation with applied external electric fields, where for the given electrical excitation a maximum electric field driven rotary domain wall motion of about 7° occurs. The magnetization response measured inside the magnetic domains shows a mostly linear change with electric field (Fig. 7(d)). Yet, at electrical fields where the magnetization response deviates from linearity, the domain wall angle stays constant over a wide range (Fig. 7(d)). The domain wall movement is non-linear with electric field excitation. Depending on the field history irreversible wall jumps are observed. The deviation from the linear response causes a hysteretic change in magnetization, possibly contributing to the noise level for ME-sensors (Fig. 7(e)).

B. Domain wall motion - MHz dynamics

Magnetic reversal in the presence of an rf magnetic field strongly depends on the magnetic field frequency. At sub-GHz frequencies the magnetization reversal may take place by domain wall motion. Dynamic MOKE imaging in the relevant frequency range is the method of choice to unambiguously identify the related magnetic processes. As an example, the change of magnetization response in a ferromagnetic thin film element that displays a magnetic Landau structure is imaged stroboscopically (Fig. 8). The static magnetic domain configuration after demagnetizing is shown

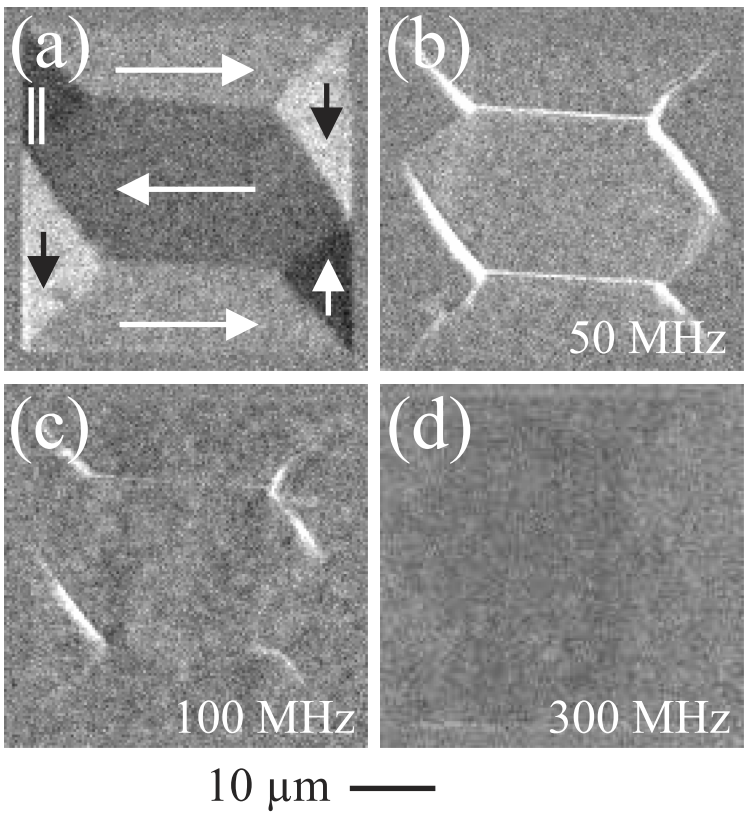

FIG. 8. (a) Static magnetic domain configuration in a 40 μm×40 μm square of $(Fe_{90}Co_{10})_{78}Si_{12}B_{10}$ amorphous ferromagnetic film with a thickness of 160 nm after demagnetizing along its easy axis of magnetic anisotropy. Differential time-resolved images during application of an excitation field with a frequency of (b) 50 MHz, (c) 100 MHz, and (d) 300 MHz. The plane of incidence is indicated in (a) (after Ref. 13).

in Fig. 8(a). Applying an excitation field with a frequency of 50 MHz, 90° domain walls move as seen from the differential dynamic MOKE image (Fig. 8(b)).[13] Fig. 8(c) displays the magnetic response to a field with a frequency of 100 MHz. As it can be seen, by increasing the field frequency the area swept by the magnetic domain walls decreases. This is attributed to the fact that at higher frequencies the domain walls cannot completely follow the field changes. Further increasing the excitation frequency to 300 MHz causes an almost complete roll-off in domain wall motion (Fig. 8(d)). From the direct MOKE imaging of domain wall movement it is possible to derive the domain wall velocity. For the sample discussed above a maximum wall velocity of $v_{DW} = 60$ m/s is obtained.[13]

C. Magnetization precession and spin waves - GHz dynamics

Unlike for the low frequency reversal, in the GHz frequency regime the magnetization reversal happens through precessional motion of magnetization. Fig. 9(a) and 9(b) show the response of the sample discussed in the previous section to an excitation at its ferromagnetic resonance frequency ($f_{res} = 3$ GHz). Precessional motion of magnetization inside the domain wall becomes directly observable. The MOKE images reveal not only uniform precession of magnetization but also inhomogeneous dynamic modes inside the domains. Besides, closure domains contribute to the dynamic response through magnetostatic inter-domain coupling through out-of-plane magnetization precession. The obtained time-resolved MOKE data can effectively be used for studying lateral flux propagation mechanisms in soft magnetic films. Based on spatially and temporally resolved MOKE imaging data in Ref. 13 a new model for high-frequency flux transfer in patterned soft magnetic elements was proposed.

Spin waves are collective excitations of magnetization in a magnetic lattice. The spin waves can be excited by different means, for instance not only by using microwave antennas,[14] but also from domain wall oscillations[15,16] and magnetic vortex reversal.[17] Here, we present a proof of the generation of spin waves from flux-closed vortex configuration via time-resolved MOKE imaging. Fig. 10(a) shows the static Kerr image of a square $Ni_{81}Fe_{19}$ element with a center vortex. As seen in Fig. 10(b), with an excitation frequency of 50 MHz oscillatory domain wall motion takes place. Increasing the magnetic field frequency to 1 GHz and 2 GHz, Fig. 10(c) and 10(d) respectively, the dynamic magnetic response behavior is shifting to be dominated by precessional motion of magnetization. The MOKE contrast mostly results from out-of-plane contributions of magnetization. Further increasing the excitation frequency to 3 GHz, signatures of spin wave appear (Fig. 10(e) and 10(f)). This is due to the excitation of spin wave modes from out-of-plane magnetization components from the central vortex.[17] The spin waves confine at higher field frequencies up to 4 GHz (Fig. 10(g) and 10(h)). Spin waves are generated from the center and propagate to the edges in a physical path determined by the 90° Néel walls. The direction of SW propagation

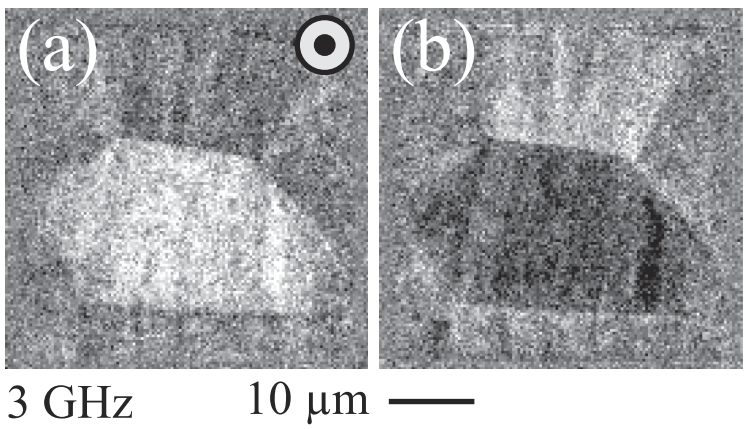

FIG. 9. Time-resolved MOKE images obtained from a $(Fe_{90}Co_{10})_{78}Si_{12}B_{10}$ sample at an excitation field with a frequency of 3 GHz at a field phase of (a) 0° and (b) 180°. All images with perpendicular incidence (⊙) as indicated in (a) (after Ref. 13).

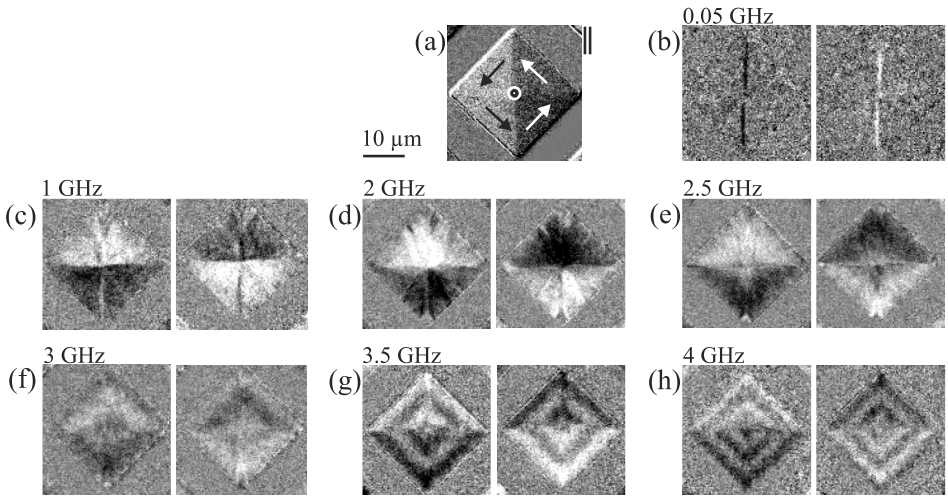

FIG. 10. (a) Static domain configuration of a 30 μm × 30 μm $Ni_{81}Fe_{19}$ element with a film thickness of 30 nm. Time-resolved MOKE images at an excitation field with a frequency of (b) 0.05 GHz (c) 1.0 GHz, (d) 2.0 GHz, (e) 2.5 GHz, (f) 3.0 GHz, (g) 3.5 GHz, and (h) 4.0 GHz. All images with oblique plane incidence (||) as indicated in (a).

is perpendicular to the magnetization, identifying them as forward volume spin wave modes. The possibility of generating spin waves from domain wall oscillations along a magnetic path constricted by 180° domain walls was discussed in detail in Ref. 15, where the tuning of the wavelength of spin waves by varying the excitation field frequency is investigated and imaged by time-resolved MOKE microscopy.

VI. BEYOND MAGNETIC DOMAIN IMAGING - TEMPERATURE IMAGING

The use of MO effects beyond magnetic domain imaging was put forward for the imaging of temperature fields.[18] Using $BiLu_2Fe_4GaO_{12}$ garnet films with a Néel temperature T_N around room temperature as a MO indicator film (MOIF), the probing of lateral varying temperature maps with high lateral as well as temporal resolution was demonstrated. Local changes in temperature are detected from the alteration of saturation magnetization of the MO active layer with temperature, which are most pronounced when the temperature approaches (but is still below) T_N of the ferrimagnetic garnet material. A plot of the magneto-optical Faraday effect (MOFE) intensity change with temperature below and above T_N is displayed in Fig. 11(a). The modifications of the MOFE signal obtained in a magnetically saturated sample can then be used as an indicator for the qualitative visualization of lateral temperature distributions. A pyro-magneto-optical imaging experiment is demonstrated in Fig. 11(b)-11(e), where temperature changes are imaged that result from a current carrying integrated circuit structure (Fig. 11(b)) with a central constriction.

Placing the temperature sensing MOIF[4] with magnetic out-of-plane anisotropy on top of the IC structure under study and with the application of a current I through the constriction, the MOIF reacts to the local magnetic field generated from the wire (Fig. 11(c)). Cylindrical domains are visible, the width of which gradually changing with distance to the wire. The magnetization is saturating inside the loop of the current carrying microwire. More important, a small reduction of MOFE domain contrast above the locally heated high resistance constriction becomes visible. The reduction in MOFE contrast already indicates a local increase in temperature. Under a magnetic saturation field aligned parallel to the out-of-plane anisotropy of the garnet layer, the magnetic domain pattern is eliminated completely (Fig. 11(d)). In this imaging mode, changes in MOFE amplitude are now solely related to local variations in temperature. Thus, the outlines of the resistive wire are visible in the spatial temperature map with the strongest intensity change at the thermal hot-spot located at the wire constriction. After calibration of the temperature dependence of the MOFE contrast, real temperature maps are derived (Fig. 11(e)). Spatial temperature changes well

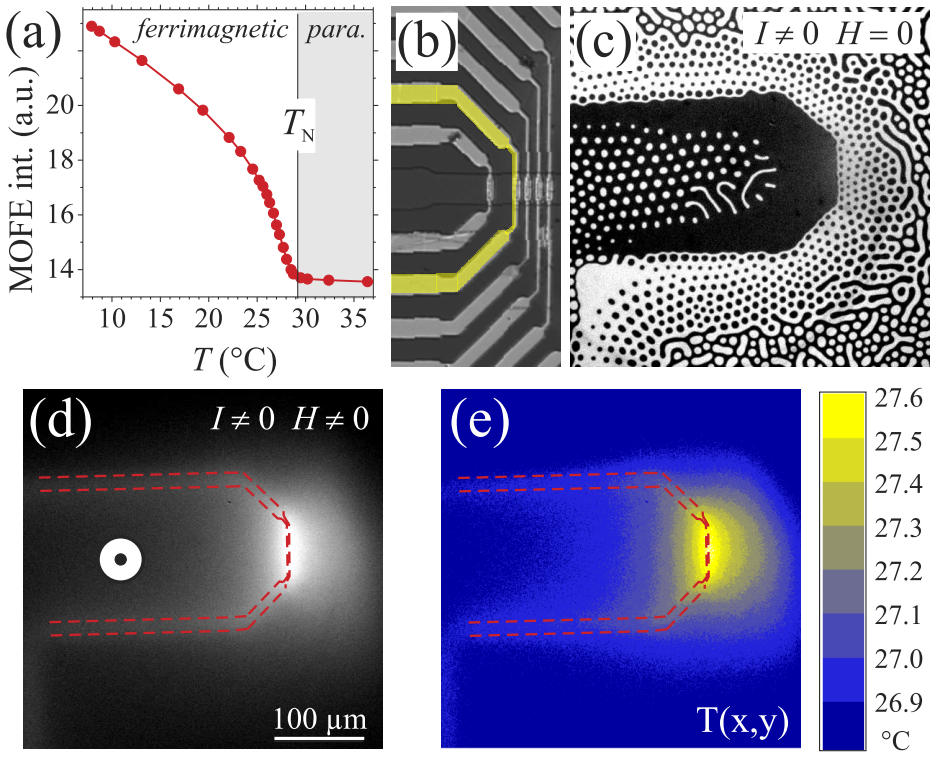

FIG. 11. (a) MOFE intensity versus temperature of a MOIF layer around the Néel temperature T_N. (b) Central microwire structure with a connected microwire with a central constriction (as marked). MOFE image with the application of current (c) without and (d) with an additionally applied out-of-plane magnetic saturating field. (e) Temperature map derived after calibrating the MOFE contrast. The outlines of the resistive microwire sketched in (d) and (e). All MOIF images are obtained with perpendicular incidence of light (polar MOFE) (adapted from Ref. 18).

below one degree Kelvin are distinguishable in the MO obtained thermal image. A temperature resolution of 0.01 K/Hz$^{0.5}$ and a temporal resolution of 1 millisecond is demonstrated in Ref. 18.

VII. CONCLUSIONS

MO microscopy using the MO Kerr effect, the MO Faraday effect, the MO Voigt effect, and the MO gradient effect provides various options for the imaging of magnetic domain structures. Using pulsed light emitting diodes, or pulsed laser illumination sources, imaging with adjustable temporal resolution down to picoseconds is achievable. Magnetic and electric field induced magnetization reversal can be visualized directly. Magnetic domain features on length scales from centimeters to sub-micrometer length scales can be imaged by the same method and at the same speed. Due to recent advances in MO microscopy like simultaneous multi-sensitivity imaging, MO microscopy will remain one of the most relevant experimental techniques for the investigation of magnetic domain behavior. MO microscopy has not yet reached its full potential.

ACKNOWLEDGMENTS

Funding from the German Science Foundation (DFG) through grants Mc9/8-3, Mc9/10-1, Mc9/10-2, Mc9/15-1, and through the Collaborative Research Centre SFB 855 “Magnetoelectric Composite Materials-Biomagnetic Interfaces of the Future” is highly acknowledged. Additional support through the Heisenberg Programme of the DFG is acknowledged (Mc9/9-1, Mc9/9-2). P.M. thanks for support through the SYMPHONY project operated within the Foundation for Polish Science within the Team Programme co-financed by the EU European Regional Development Fund,

Grant No. OPIE 2007-2013 and the FUGA project financed by the Polish National Science Centre, DEC-2015/16/S/ST3/00450.

[1] A. Hubert and R. Schäfer, *Magnetic Domains - The Analysis of Magnetic Microstructures* (Springer, Berlin, 1998).
[2] M. R. Freeman and B. C. Choi, Science **294**, 1484 (2001).
[3] P. Fischer, Materials Science and Engineering R-Reports **72**, 81 (2011).
[4] J. McCord, Journal of Physics D: Applied Physics **48**, 333001 (2015).
[5] T. von Hofe, N. Onur Urs, B. Mozooni, T. Jansen, C. Kirchhof, D. E. Bürgler, E. Quandt, and J. McCord, Applied Physics Letters **103**, 142410 (2013).
[6] R. Schäfer, C. Hamann, J. McCord, L. Schultz, and V. Kamberský, New Journal of Physics **12**, 053006 (2010).
[7] R. Schäfer and A. Hubert, physica status solidi (a) **118**, 271 (1990).
[8] A. Maziewski, P. Mazalski, Z. Kurant, M. O. Liedke, J. McCord, J. Fassbender, J. Ferré, A. Mougin, A. Wawro, L. T. Baczewski, A. Rogalev, F. Wilhelm, and T. Gemming, Physical Review B **85**, 054427 (2012).
[9] V. Röbisch, E. Yarar, N. O. Urs, I. Teliban, R. Knöchel, J. McCord, E. Quandt, and D. Meyners, Journal of Applied Physics **117**, 17 (2015).
[10] A. Piorra, R. Jahns, I. Teliban, J. L. Gugat, M. Gerken, R. Knöchel, and E. Quandt, Applied Physics Letters **103**, 032902 (2013).
[11] R. Jahns, H. Greve, E. Woltermann, E. Quandt, and R. Knöchel, Sensors and Actuators A: Physical **183**, 16 (2012).
[12] N. O. Urs, I. Teliban, A. Piorra, R. Knöchel, E. Quandt, and J. McCord, Applied Physics Letters **105**, 202406 (2014).
[13] B. Mozooni, T. von Hofe, and J. McCord, Physical Review B **90**, 054410 (2014).
[14] M. Bailleul, D. Olligs, C. Fermon, and S. O. Demokritov, EPL (Europhysics Letters) **56**, 741 (2001).
[15] B. Mozooni and J. McCord, Applied Physics Letters **107**, 042402 (2015).
[16] J. Mullenix, A. El-Ghazaly, D. W. Lee, S. X. Wang, and R. M. White, Physical Review B **89**, 224406 (2014).
[17] M. Kammerer, M. Weigand, M. Curcic, M. Noske, M. Sproll, A. Vansteenkiste, B. Van Waeyenberge, H. Stoll, H. B. C. Woltersdorf, Georg, and G. Schuetz, Nature Communications **2**, 279 (2011).
[18] M. Kustov, R. Grechishkin, M. Gusev, O. Gasanov, and J. McCord, Advanced Materials **27**, 5017 (2015).